DOI: 10.1002/ejic.200600271

Bifunctional Materials Based on the Photochromic Cation $[RuNO(NH_3)_5]^{3+}$ with Paramagnetic Metal Complex Anions

Lyudmila A. Kushch,*[a] Lyudmila S. Kurochkina,[a] Eduard B. Yagubskii,[a] Gennadii V. Shilov,[a] Sergei M. Aldoshin,[a] Vyacheslav A. Emel'yanov,[b] Yurii N. Shvachko,[c] Vladimir S. Mironov,[d] Dominik Schaniel,[e] Theo Woike,[e] Chiara Carbonera,[f] and Corine Mathonière[f]

Keywords: Photochromism / Magnetic properties / Mononitrosyl ruthenium complexes / Paramagnetic metal complexes

The synthesis of a series of compounds containing the photochromic mononitrosyl cation, $[RuNO(NH_3)_5]^{3+}$ and metal complex paramagnetic anions $[M(CN)_6]^{3-}$ [M = Cr (**1**), Fe(**2**)], $[M(ox)_3]^{3-}$ [M = Cr(**3**), Fe(**4**)] and $[CrNO(CN)_5]^{3-}$ (**5**) is reported. The crystal structures of the salts **1** and **3** are discussed. In contrast to **1** and **3** which exhibit reversible photochromic properties, illumination of **2** and **4** results in an irreversible photochemical reaction and compound **5** is not photochromic at all. The magnetic properties of **1** and **3** have been investigated and complex **1** shows a weak reversible increase in the value of $\chi_M T$ under light irradiation at low temperature.

Introduction

Over the last decade new types of molecular based magnets, namely functionalised magnets with combined magnetic and optical properties, have been studied extensively.[1–4] Current research in this field is focused not only on the improvement of magnetic properties but also on the search for unusual properties which have not been realised in magnets so far. In 1996, low-temperature photoinduced magnetisation was discovered in the prussian blue analogue $K_{0.2}Co_{1.4}[Fe(CN)_6]\cdot 6.9H_2O$.[1] The design of such bifunctionalised molecular materials with reversible modifications of their magnetic properties makes it possible to control magnetic properties by an external stimulus (light) and this opens up the possibility for technical applications in displays, information and energy storage devices and sensors.[5]

Up to now several strategies exist, using different types of light-sensitive building blocks, for producing the photomagnetic effect in molecular compounds combining magnetic and optical properties.[5] One of the approaches uses anionic photochromic mononitrosyl complexes of transition metals as light-sensitive units in the synthesis of bifunctionalised magnetic materials. This was successfully shown with $Ni[FeNO(CN)_5]$. The nitroprusside anion is diamagnetic but exhibits a photoinduced transition to two extremely long-lived metastable states, MSI and MSII, by irradiation with light in the blue-green spectroscopic range (350–580 nm) at temperatures below 180 K.[6,7] In $Ni[FeNO(CN)_5]$, randomly aligned neighbouring Ni^{II} spins with $S = 1$ are ordered after excitation to MSI via two antiferromagnetically coupled spins formed by charge transfer from the Fe atom to the NO ligand. These spins induce magnetic coupling between the neighbouring Ni cations followed by the formation of a magnetic cluster with $S = 5$.[2a,2c]

Recently, it has been found that cationic mononitrosyl Ru complexes also exhibit photochromic properties. Like the anionic mononitrosyl complexes, the cationic Ru species exhibit two long-lived metastable states. MSI can be generated by light irradiation in the blue-green spectroscopic range (350–580 nm), while MSII can be obtained by subsequent illumination in the blue-green and infrared spectroscopic ranges (e.g. 1064 nm). In these Ru complexes, the metastable states have higher decay temperatures (up to +20 °C for MSI and up to –45 °C for MSII).[8–10]

It was of interest to use the photochromic mononitrosyl Ru cation as a light-sensitive building block for synthesising bimetallic compounds with paramagnetic anions.[11] Here we report the preparation, structures, photochromic and magnetic properties of bimetallic complexes containing the

[a] Institute of Problems of Chemical Physics, RAS, MD142432 Chernogolovka, Russia
E-mail: lkushch@icp.ac.ru
[b] Institute of Inorganic Chemistry, Siberian Division of RAS, 630090 Novosibirsk, Russia
[c] Institute of Metal Physics Ural Division, RAS, GSP-170, 620219 Ekaterinburg, Russia
[d] A.V. Shubnikov Institute of Crystallography, RAS, 117333 Moscow, Russia
[e] Institut für Mineralogie, Universität zu Köln, Zülpicherstrasse 49b, 50674 Köln, Germany
[f] Groupe des Sciences Moléculaires, University of Bordeaux 1, Institut de Chimie de la Matière Condensée de Bordeaux, UPR CNRS 9048, 33608 Pessac Cedex, France

photochromic cation $[RuNO(NH_3)_5]^{3+}$ and the paramagnetic metal complex anions $[M(CN)_6]^{3-}$, [M = Cr(**1**), Fe(**2**)], $[M(ox)_3]^{3-}$ [M = Cr(**3**), Fe(**4**)] and $[CrNO(CN)_5]^{3-}$(**5**). The influence of light on the magnetic properties of $[Ru(NH_3)_5NO][Cr(CN)_6]$ has been studied. A weak increase in the value of $\chi_M T$ under light irradiation at low temperature has been observed.

Results and Discussion

Synthesis and Structural Characterisation

The following series of salts, comprised of the mononitrosyl photochromic cation of $[RuNO(NH_3)_5]$ and paramagnetic anions, was synthesised by metathesis in water: $[RuNO(NH_3)_5][Cr(CN)_6]$ (**1**), $[RuNO(NH_3)_5][Fe(CN)_6]$ (**2**), $[RuNO(NH_3)_5][Cr(ox)_3]\cdot 3H_2O$ (**3**), $[RuNO(NH_3)_5][Fe(ox)_3]\cdot xH_2O$ ($x \approx 3$) (**4**) and $[RuNO(NH_3)_5][CrNO(CN)_5]$ (**5**).

The crystal structures of **1**–**5** were investigated. Compound **2** is isostructural with **1** whereas **4** is not isostructural with **3**. The complete structural solutions of **2**, **4** and **5** are currently in progress. The main crystallographic data for **1** and **3** are presented in Table 1 and the crystal structure of **1** has been briefly published in ref.[11] The structure is formed from two independent structural units, i.e. $[RuNO(NH_3)_5]^{3+}$ and $[Cr(CN)_6]^{3-}$. The Ru and Cr atoms lie on a threefold axis and alternate along the *c* axis (Figure 1). There are numerous N···N contacts [2.93–3.23(2) Å] between the CN ligands of the anion and the NH_3 ligands of the cation. The occurrence of the N···N contacts is apparently due to the existence of C–N···H–N hydrogen bonds between complex components. The cations and anions located on the same threefold axis are coupled to each other by three hydrogen bonds. However, each cation and anion pair is linked by hydrogen bonds with three neighbouring cations and anions located on neighbouring threefold axes. It should be noted that the anion and cation from a pair are always linked with the cation and anion from different pairs, which results in the formation of a 3D network of hydrogen bonds in the crystal.

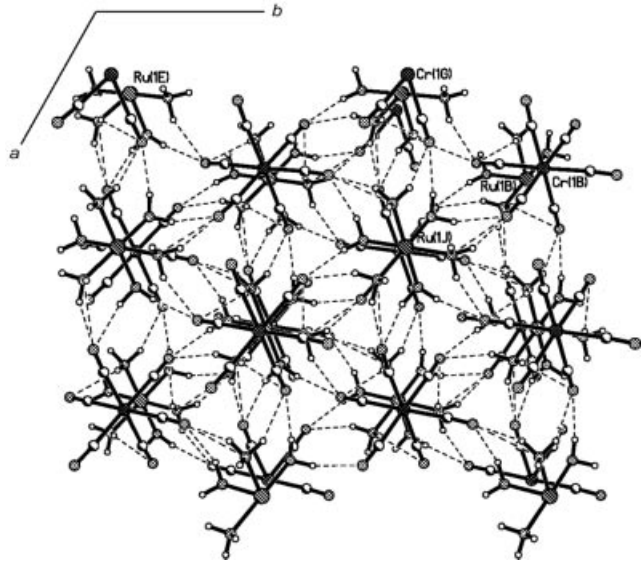

Figure 1. Projection of the crystal structure of **1** on the *ab* plane.

It should be especially emphasised that some anomalies can be observed in the structure of **1**: (a) the Ru–N–O linkage in the $[RuNO(NH_3)_5]^{3+}$ cations is bent (ca. 155°) and

Table 1. Crystal data and structure refinement for **1** and **3**.

Compound	$[RuNO(NH_3)_5][Cr(CN)_6]$(**1**)	$[RuNO(NH_3)_5][Cr(C_2O_4)_3]\cdot 3H_2O$(**3**)
Formula	$C_6H_{15}CrN_{12}ORu$	$C_6H_{21}CrN_6O_{16}Ru$
*F*w	424.37	586.36
Temp. [K]	293(2)	293(2)
Radiation λ [Å]	0.71069	0.71069
Crystal size [mm]	0.08×0.1×0.35	0.15×0.15×0.50
Crystal system	hexagonal	hexagonal
Space group	*R*3	$P\bar{3}1c$
a [Å]	11.224(2)	12.613(2)
b [Å]	11.224(2)	12.613(2)
c [Å]	10.957(2)	20.652(4)
α [°]	90	90
β [°]	90	90
γ [°]	120	120
V [Å^3]	1195.4(4)	2845.3(8)
Z	3	6
$\rho_{calcd.}$ [g cm^{-3}]	1.768	1.864
μ, [cm^{-1}]	1.643	1.442
Reflections collected	1926	7491
Independent reflections	1244	2534
[$I > 2\sigma I$]	681	2009
θ range [°]	2.80–40.08	1.86–30.10
GOOF	0.928	0.906
R	0.1151	0.0588
R_1	0.0377	0.0491
wR_2	0.1009	0.1009
abs. structure Flack	–0.29(16)	–

(b) the Cr–C distances differ considerably (ca. 0.1 Å) in the $[Cr(CN)_6]^{3-}$ hexacyano anion. This deserves a special comment. In the ground state of mononitrosyl Ru^{II} complexes such as $[RuNO(NH_3)_5]Cl_3 \cdot H_2O$,[13,24] $Na_2[RuNO(CN)_5]$,[14] $K_2[RuNOCl_5]$[21] and $K_2[RuNOBr_5]$[22] containing the positively charged $(NO)^+$ ligand, the M–N–O group is normally linear although a strongly bent M–N–O geometry (ca. 90°) may be observed in the photoexcited metastable MSII state in some of these complexes. Related six-coordinate iron(II), osmium(II) and some other mononitrosyl complexes such as $[Ni(NO)(\eta^5\text{-Cp})]$ show similar behaviour.[13] However, in complexes with a neutral NO ligand the M–N–O group is often strongly bent even in the ground state.[13,15,16] This is due to the role of the antibonding π*(NO) orbital of the NO ligand. According to the classification scheme of Feltham and Enemark,[17] the M–N–O bond angle in transition-metal nitrosyl complexes is defined by a total number of electrons, *n*, in the metal ion M and the π*(NO) orbital. For six-coordinate (pseudo-octahedral) mononitrosyl complexes, the M–N–O angle is 180 ± 10° for $n \leq 6$, 145 ± 10° for $n = 7$ and 125 ± 10° for $n = 8$. These data are consistent with quantum chemical calculations.[18,19]

The nonlinear ground-state geometry of the Ru–N–O group in $[RuNO(NH_3)_5]^{3+}$ is unusual since a study of the optical properties of **1** showed the NO group to be positively charged ($\tilde{\nu}_{NO}$ = 1947 and 1914 cm^{-1}). On closer inspection, however, this can naturally be rationalised in terms of attractive coulombic interactions between NO^+ and CN^- groups (having opposite electrical charges) combined with the specific crystal structure of **1**, as illustrated in Figure 2. In the room-temperature crystal structure of **1**, the nitrosyl groups are statistically disordered in three equivalent positions. Therefore, the occupancy in the refined structure was assumed to be equal to ⅓ for the NO ligand and ⅔ for the corresponding NH_3 groups. However, regardless of the specific location of the NO^+ group in the "frozen rotation" configuration of the $[RuNO(NH_3)_5]^{3+}$ cations, the positively charged nitrosyl group (N1c and O1c atoms, Figure 2) is always in contact with five negatively charged cyano groups from three $[Cr(CN)_6]^{3-}$ anions, Figure 2. The environment of the O1c atom is symmetric enough: five contacts form a square bipyramid (contacts of the O1c atom with N4o, N3s, N4c, N4w, and N3g atoms, shown in solid grey lines). The resultant coulombic force is directed towards the N3g atom (black downward arrow). The environment of the nitrogen N1c atom of the nitrosyl group is less symmetric and consists of two short contacts [N1c–N3s 3.00(2) Å and N1c–N4o 3.09(2) Å] and two long contacts [N1c–N4w 3.58(2) Å and N1c–N4c 3.57(2) Å black lines]. The fifth contact (with the N3g atom) is absent. Since the positive electrical charge of the nitrosyl group is preferentially concentrated on the N1c atom (due to lower electronegativity), this atom is attracted to the two nitrogen atoms of two cyano groups with short contacts (N1c–N3s and N1c–N4o, two thin arrows, Figure 2). The resultant coulombic force should be directed approximately to the midpoint of the N3s–N4o line (this force is shown with a bold and long black arrow in Figure 2). As a consequence, two coulombic forces at O1c and N1c make a torsional moment which bends the Ru1c–N1c–O1c bond. Note that at such short distances (3.0–3.5 Å), attractive coulombic interactions are quite strong (ca. 2–4 eV, depending on effective charges on the actual atoms) resulting in such a pronounced distortion in the Ru–N–O bond angle (ca. 25°). Note that

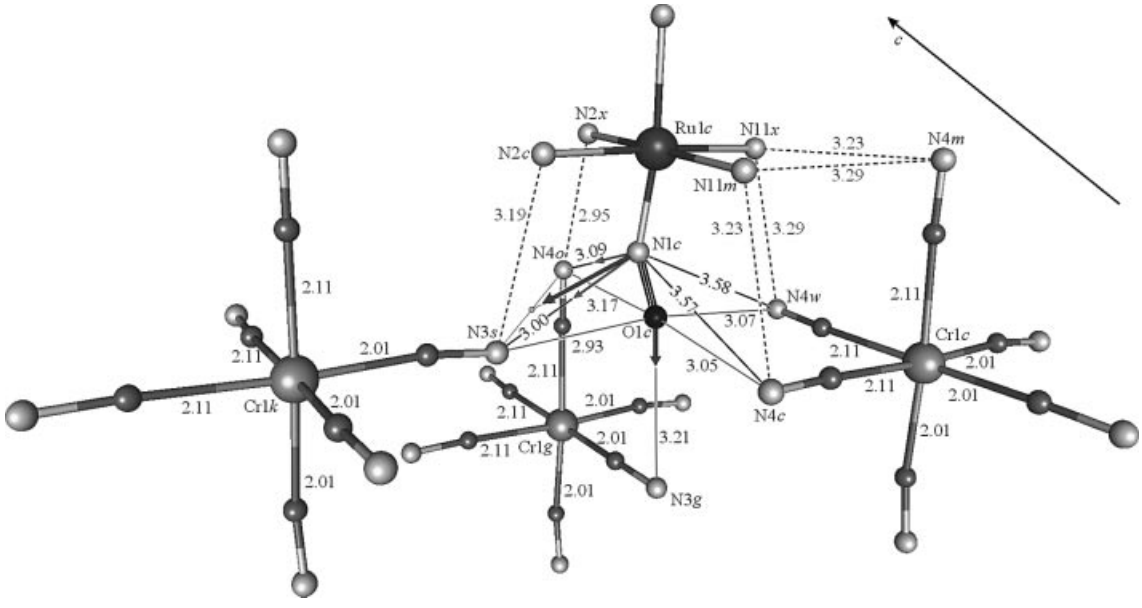

Figure 2. Immediate environment of the nitrosyl group (O1c and N1c atoms) in the 'frozen' orientation of the $[RuNO(NH_3)_5]^{3+}$ cation is drawn in perspective. The coulombic forces acting on the N1c and O1c atoms of the nitrosyl group are shown by arrows. Some of the H···N hydrogen bonds between H atoms of the NH_3 ligands of the $[RuNO(NH_3)_5]^{3+}$ cations and N atoms of the cyano groups of the $[Cr(CN)_6]^{3-}$ anions are shown with grey dashed lines as contacts between the N atoms of NH_3 ligand (N2c, N2x, N11m, and N11x, hydrogen atoms are not shown) with N atoms of the cyano groups (N4o, N3s, N4c, N4w, and N4m). Short (2.01 Å) and long (2.11 Å) Cr–C bonds of the $[Cr(CN)_6]^{3-}$ anions are indicated (the errors in length bonds do not exceed 0.02 Å).

the azimuthal orientation of the Ru1c–N1c–O1c plane is consistent with local geometry conditions for the coulombic forces shown in Figure 2. Therefore, despite rather limited accuracy in the refinement of the N–O position in the X-ray analysis of **1**, these arguments strongly support the existence of a bent Ru–N–O geometry. Furthermore a similar bent Ru–N–O ground-state structure (ca. 160°) was previously observed in the molecular compound $(BETS)_2[RuNOBr_5]$.[20] This anomaly was explained by the change in the effective charge on the nitrosyl ligand due to partial transfer of electron density from the organic BETS molecules. However, similar to the case of **1**, this can also be rationalised in terms of attractive coulombic attractions between the NO^+ group and the S centre of the BETS molecules and with Br^- ligands of neighbouring $[RuNOBr_5]^{2-}$ anions. Interestingly, in the related complex $(BETS)_2[RuNOCl_5]$, the Ru–N–O group is almost linear (178°). This could be due to the differences in the specific geometry of $Ru–NO^+\cdots X^-$ contacts (distances, bond angles) in $(BETS)_2[RuNOX_5]$ (X = Cl, Br) which have different crystal structures. In the case of X = Br, the $NO^+–X^-$ attractive interactions seem to be stronger than in the case of X = Cl. Qualitatively, this is consistent with the fact that in the compound with X = Br the NO^+ group occupies only one crystallographic position, while in compound with X = Cl the NO^+ group is disordered between two positions. In contrast to $(BETS)_2[RuNOX_5]$ compounds, the Ru–N–O bond angles are almost linear in the precursor compounds $K_2[RuNOBr_5]$ and $K_2[RuNOCl_5]$, i.e. 174.4(1)° for X = Br and 176.7(5)° for X = Cl.[21,22] These observations indicate that in some molecular compounds with $[RuNOX_5]^{2-}$ building blocks, external interactions can strongly affect the Ru–N–O bond angle. This effect is sensitive to the specific crystal structure.

The second anomaly is associated with the distortion of the octahedral $Cr(CN)_6^{3-}$ anion. The Cr–CN bonds are essentially different, three of them are 2.01(1) Å and the other three are 2.11(1) Å (Figure 2). The C(2)–Cr(1)–C(2) angles are 87.3(2)° and the C(1)–Cr(1)–C(1) angles are 92.3(2)° (Figure 3). The origin of this structural anomaly in the $[Cr(CN)_6]^{3-}$ anions is less evident. In contrast to the case of the nitrosyl group, the immediate environment of the CN group can vary depending on the specific orientation of the NO^+ groups in the closest $[RuNO(NH_3)_5]^{3+}$ cations. These may rotate about the C_3 axis by 120° and many local configurations are therefore possible. An example of the local crystal structure around the CN^- group is shown in Figure 3. The cyano group (N3 and C1 atoms in Figure 3) is involved in several $CN\cdots NH_3$ and $NO^+\cdots CN^-$ contacts with $[RuNO(NH_3)_5]^{3+}$ cations lying in the same Ru–Cr–Ru chain (running along the *c* axis, Figure 3) and in the neighbouring chains. Within each specific Ru–Cr–Ru chain, the cyano groups in contact with NO^+ groups (such as C2–N4 and C2b–N4b cyano groups in Figure 3) have considerably longer Cr–C bonds [2.11(1) Å] compared with those [2.01(1) Å] for cyano groups in contact only with NH_3 ligands (such as the C1–N3 and C1a–N3a cyano groups in Figure 3). This is unusual because in many molecular compounds containing $[Cr(CN)_6]^{3-}$, the octahedra are slightly distorted with the Cr–C distances fluctuating typically around 2.06 ± 0.03 Å.[23] Therefore, a pronounced difference in the Cr–C bond lengths indicates a strong perturbing effect of the $CN\cdots H(NH_3)$ hydrogen bonds and $NO^+\cdots CN^-$ coulombic attractions (they are comparable in magnitude). This implies that the actual "frozen" structure of the $[Cr(CN)_6]^{3-}$ anions can be considerably different from the statistically averaged crystallographic structure of C_{3v} symmetry. In particular, some of the Cr–C bonds to the CN groups in contact with the NO^+ ligand of $[RuNO(NH_3)_5]^{3+}$ are even longer than 2.11 Å. Similarly, some of the Cr–C bonds of CN groups in contact with the NH_3 ligand may be shorter than 2.01 Å. This can cause a large zero-field splitting of the $^4A_{2g}$ ground spin state of the $[Cr(CN)_6]^{3-}$ anion (see below).

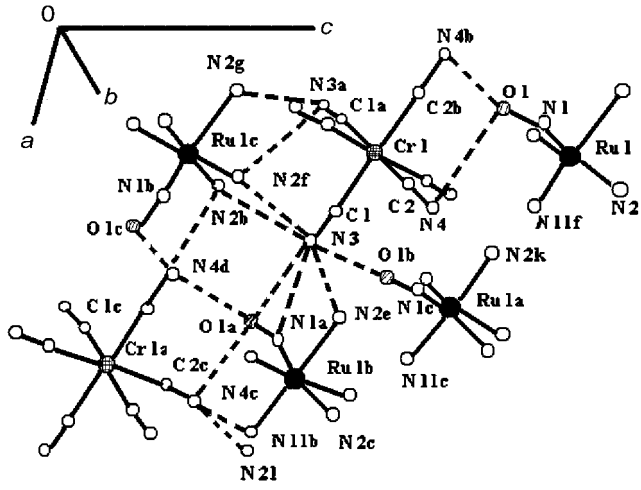

Figure 3. Fragment of the crystal structure of **1**. The threefold axes run through Ru(1), Cr(1), Ru(1c) and Cr(1a), Ru(1b), Ru(1a). The dotted lines show N···N and N···O contacts between CN ligands of the anions and NH_3 and NO ligands of the cations. The hydrogen atoms have been omitted for clarity.

An X-ray analysis of **3** showed that the crystal structure is formed from two types of $[RuNO(NH_3)_5]$ cations, $[Cr(ox)_3]$ anions and two types of water molecules. In two of the six $[Ru(1)NO(NH_3)_5]$ cations (Ru1) arranged in the unit cell, the NO group is disordered over six positions and in the other four $[Ru(2)NO(NH_3)]$ cations (Ru2) it is disordered over three positions (Figure 4, a). The Ru–N–O angle in Ru1 is 170(3)°, while in Ru2 it is equal to 178.5(2)°. Other valence angles and bond lengths in both types of cation are close to those found in **1** and $[RuNO(NH_3)_5]Cl_3·H_2O$.[24] In two $[Cr(1)(C_2O_4)_3]$ (Cr1) anions all six Cr(1)–(O1) distances are 1.986(2) Å, while in four $[Cr(2)(C_2O_4)_3]$ (Cr2) groups the Cr–O distances are somewhat longer, namely, 2.017(2) and 2.013(2) Å. There are two different water molecules in the structure: one of them is in a general position (O7) and the other one is in a special position (O8). The water molecule (O8) is orientationally disordered. There are many shortened N···O and O···O contacts between cations, anions and water molecules. As in **1**, the occurrence of short N···O and O···O contacts is apparently due to the existence of

a net of N–H···O, N–O···O and O–H···O hydrogen bonds between the components of the complex (Figure 4, a and b). Ru1 cations are linked to Cr1 anions by five hydrogen bonds [intermolecular N(1)···O(1) contacts of 2.89(2) Å]. Instead of a sixth hydrogen bond, a shortened van der Waals O(11)···O(1) contact equal to 2.74(2) Å can be observed. A shorter contact O(11)···O(21) [2.47(2) Å] can be observed between the Ru1 and Ru2 cations (Figure 4, a). The Ru2 cations are linked by N(3)–H···O(2) hydrogen bonds with the Cr1 anion and intermolecular N(3)–H···O(2) contacts of 2.87(2) Å. The Cr1 and Cr2 anions are linked to each other by O(7) water molecules along the *c*

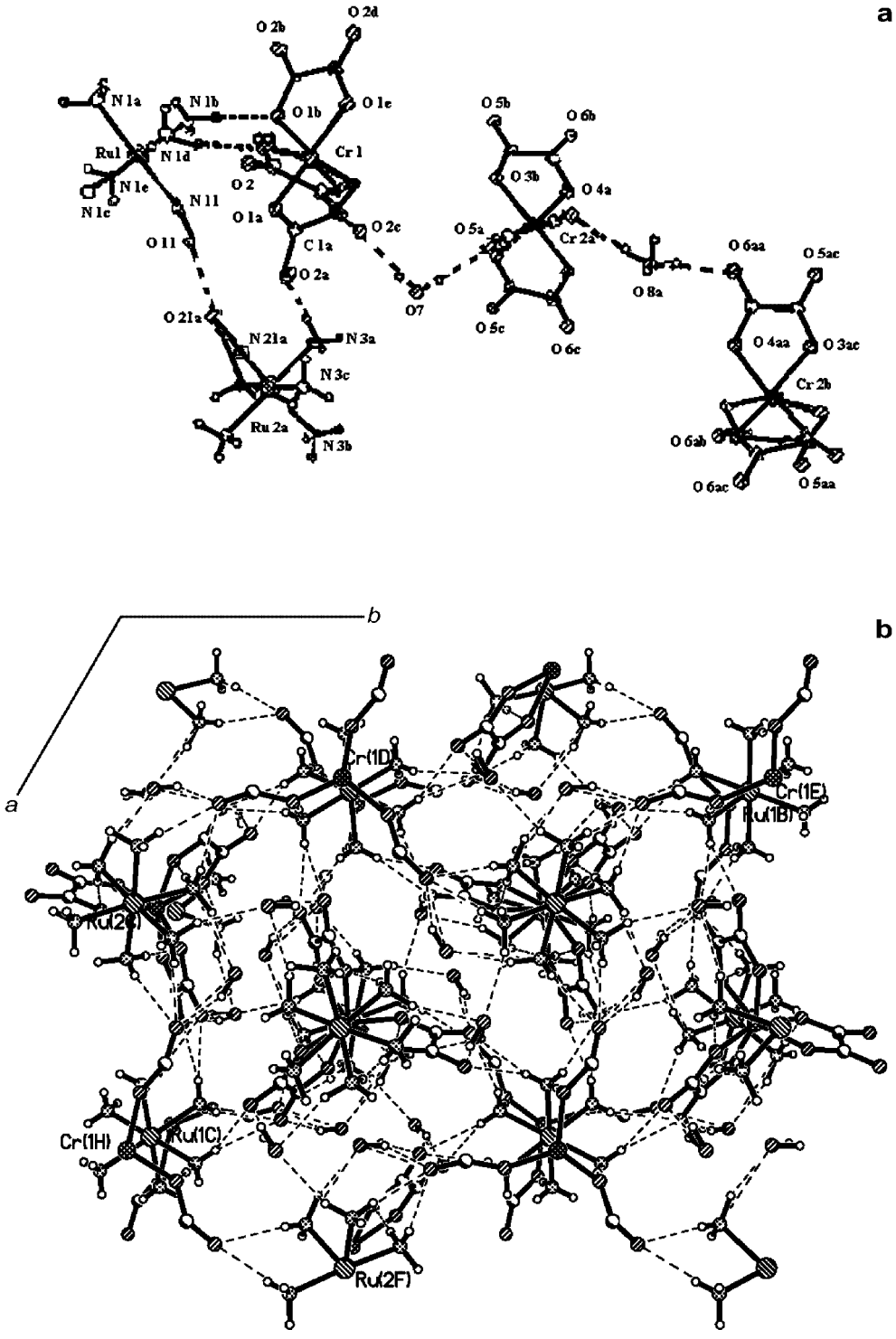

Figure 4. a) Fragment of the crystal structure of **3**. The dotted lines show O···N and O···O contacts between oxalate ligands of the anions and NH_3 and NO ligands of the cations and water molecules. The *c* axis runs parallel to the line connecting Ru(1) and Cr(1). b) Projection of crystal structure of **3** on the *ab* plane.

axis [intermolecular O(2)···O(7) and O(7)···O(5) contacts of 2.86(2) Å and 2.95(2) Å, respectively]. The O(8) water molecule links Cr2 [O(8)···O(6)–2.88(2) Å] anions in the same direction (Figure 4, a). It should be noted that the carboxyl oxygen atoms of the Cr2 anions do not participate in the formation of the hydrogen bonds, which is distinct from Cr1. This is probably the reason for the distinction between the Cr–O bond lengths in the Cr1 and Cr2 anions.

Differential Scanning Calorimetry

The photochromic properties of compounds **1**–**5** were investigated by differential scanning calorimetry (DSC). This technique has already been used to detect the existence of metastable states in complexes containing the nitroprusside anion[25,26] and some ruthenium mononitrosyl anionic[27,28] and cationic complexes.[29] With DSC we can determine the amount of energy, which heats the lattice during the thermal decay of metastable states. In contrast to mononitrosyl anionic complexes of transition metals, one exothermal peak was detected in **1** and **3** after their illumination with blue light (Figure 5).

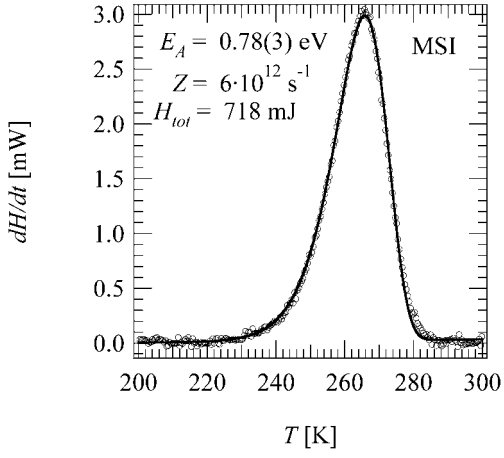

Figure 5. Thermal decay spectra (q = 5 K min^{-1}) of $[RuNO(NH_3)_5][Cr(CN)_6]$ after irradiation at 120 K with λ = 434 nm for MSI.

The appearance of the exothermal heatflow is associated with the transition of a photochromic cation from the metastable MSI state to the ground state (GS). The temperatures of the peak maxima observed in the spectra of these complexes are very close to that of $[RuNO(NH_3)_5]Cl_3{\cdot}H_2O$ (ca. 260 K).[30] It should be noted that the intensity of the DSC signal in **3** was essentially lower than that in **1**. Since the area under the heatflow curve is proportional to the number density of cations in the metastable state, this is evidence of a low population in **3**. This is possibly due to a small penetration depth of light into the "oxalate" complex crystals, which are deep-brown in colour in contrast to the light-orange crystals of **1**.

It is known that the illumination of anionic photochromic complexes by NIR light (1064 nm) transforms MSI to MSII. Recently, it was shown that subsequent irradiation of $[RuNO(NH_3)_5]Cl_3{\cdot}H_2O$ by light with wavelengths of 400–500 nm and 1000–1200 nm transfers MSI into MSII. The decay of MSII occurs at 220 K.[30] By irradiation of **1** in a manner completely analogous to $[RuNO(NH_3)_5]Cl_3{\cdot}H_2O$ this second metastable state was also detected (Figure 6).

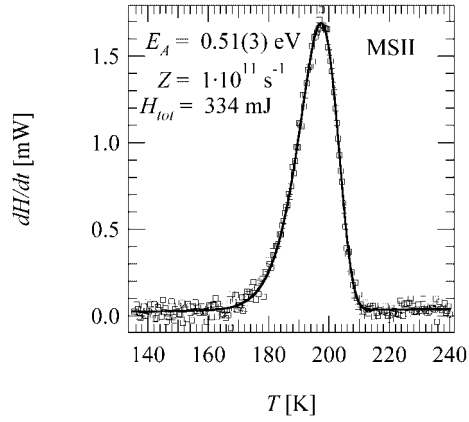

Figure 6. Thermal decay spectra (q = 5 K min^{-1}) of $[RuNO(NH_3)_5][Cr(CN)_5]$ after irradiation at 120 K with λ = 434 nm and λ = 1064 nm for MSII.

It should be noted that the decay temperature of MSII in **1** (T_d = 195 K) is 25 K lower than in the starting complex $[RuNO(NH_3)_5]Cl_3{\cdot}H_2O$ (T_d = 220 K). A possible explanation for this significant temperature reduction may be given by the structural peculiarities presented in Figure 2 and discussed above in terms of coulombic interactions. The generation of the metastable states implies that these attractive forces are overcome or at least neutralised. This may occur by means of the charge transfer from the ground state to the light-induced intermediate state π*(NO), in which the new charge distribution of the NO ligand reduces the attractive forces. During the lifetime of this intermediate state, the motion of the NO ligand is quasi-free and is finally stabilised in the new relaxed electron density distribution of the NO ligand. The same arguments apply to the generation of MSI. The key feature which allows the rotation of the NO ligand is the new charge configuration in the intermediate π*(NO) state in order to overcome the coulombic interactions. Otherwise no rotation could occur and the metastable states would not be occupied.

Since the decay of the metastable states is mono-exponential over time under isothermal conditions, the depopulation processes are first-order reactions and can be conveniently described by the Arrhenius law (see Exp. Sect.). In the present case, a fit of the experimental data allowed us to evaluate the activation energy (E_a) and the frequency factor (Z) for MSI and MSII in **1**. We obtained E_a = 0.78(3) and 0.51(3) eV, and $Z = 6\times10^{12}$ and 5×10^{11} s^{-1} for MSI and MSII, respectively. The error in the frequency factor is one order of magnitude due to the small temperature range of the measurements. These high activation energies are within the range of those determined for $[RuNO(NH_3)_5]Cl_3{\cdot}H_2O$ [E_a = 0.73(3) eV, E_a = 0.66(3) eV; $Z = 1\times10^{12}$ s^{-1}, $Z = 1\times10^{12}$ s^{-1}][31] and account for the stability of the induced metastable states at low temperature.

Complexes **2**, **4** and **5** have also been investigated by the DSC method. In contrast to **1** and **3**, which exhibit reversible photochromic properties, the illumination of **2** and 4, both of which are comprised of $[Fe(CN)_6]^{3-}$ and $[Fe(ox)_3]^{3-}$ anions, results in an irreversible photochemical reaction related to a partial reduction of Fe^{3+} to Fe^{2+}. The IR spectrum of a photoproduct of **2** shows a new band near 2044 cm^{-1} attributed to valence vibrations of the CN^- group bound to Fe^{2+}.

The DSC signal was not observed in **5** with the $[CrNO(CN)_5]^{3-}$ anion. Possibly, the X-ray analysis of the crystal structure of **5** clarifies the reason for the absence of photochromic properties. Thus, the study of the photochromic properties of **1**–**5** shows that the nature of the paramagnetic metal complex anion strongly affects the photochromism of mononitrosyl Ru complexes.

Magnetic Properties

Figure 7 shows the temperature dependence of the reciprocal paramagnetic susceptibility, χ_P^{-1}, for $[RuNO(NH_3)_5][Cr(ox)_3]\cdot 3H_2O$. The measurements were carried out at Field Cooling (FC) and $B = 10000$ G. A fit with the Curie–Weiss law, $\chi_P = C/(T - \Theta)$, with $C = 1.98$ emu K mol^{-1} and $\Theta = 0.26$ K is in good agreement with experiment down to 1.8 K. The low-temperature part of the curve is depicted in the inset. Figure 8 shows the temperature evolution of χ_P^{-1} for $[RuNO(NH_3)_5][Cr(CN)_6]$ obtained under similar experimental conditions. The data are well described by the Curie–Weiss law with $C = 1.86$ emu K mol^{-1} and $\Theta = 0.18$ K. Several experimental points at $T < 5$ K shown on the inset slightly deviate from the fitting curve. At 300 K χ_P values for **1** and **3** are equal to 6.07×10^{-3} and 6.25×10^{-3} emu mol^{-1}, respectively. A positive Θ value is usually indicative of ferromagnetic correlations, though for $S \geq 1$ such small values of Θ might also come from the zero-field splitting of the ground spin state, D. For a system of noninteracting spins with zero-field splitting, the average molar paramagnetic susceptibility χ_P shows an effective Weiss temperature Θ at $T > |D|/\kappa$ (due to interplay of perpendicular and parallel components). At $T < |D|/\kappa$, χ_P^{-1} deviates from the Curie–Weiss law. The Curie constants C for both complexes are very close to 1.88 emu K mol^{-1}, which is characteristic of noninteracting $S = 3/2$ spins. Thus, the paramagnetism of both complexes can be attributed to the Cr^{3+} spin system. No indications of the presence of a paramagnetic Ru^{III} ($S = 1/2$) oxidation state were found. The temperature behaviour of μ_{eff} for both complexes [where $\mu_{eff} = (3\kappa\chi_P T/\mu_0 N_A)^{1/2} = 2.828(\chi_P T)^{1/2}$] is presented Figure 9. The magnetic moment μ_{eff} of both complexes is little affected in the temperature range from 300 K to 5 K. Below 5 K, μ_{eff} of $[RuNO(NH_3)_5][Cr(CN)_6]$ reveals a pronounced decrease from 3.83 to 2.91 μ_B (at 1.99 K) whereas μ_{eff} of $[RuNO(NH_3)_5][Cr(ox)_3]\cdot 3H_2O$ remains nearly constant. In Figure 10 the magnetisation data in terms of magnetic moment M in Bohr magnetons ($N_{A\mu B}$) are plotted against the reduced variable B/T (in T/K). The diamagnetic response of the gel capsule has been subtracted. Samples of **1** and **3** were frozen in fields of 3 T and 5 T, respectively. Experimental points were obtained by decreasing the field to 0 at constant temperatures of 2.00 K and 1.83 K. Maximum values are 2.70 (5 T) and 2.20 (3 T), respectively. The field dependence for $[RuNO(NH_3)_5][Cr(ox)_3]\cdot 3H_2O$ is consistent with the model of noninteracting spins. A solid line corresponds to the Brillouin function with $S = 3/2$ and $g = 2.080$. The enhanced g value might be due to the ligand field splitting effect. The low-temperature behaviour of $[Cr(CN)_6]^{3-}$ anions in **1** is quite unusual and cannot be explained in terms of the Brillouin function. At higher fields ($B > 5000$ G) the effective spin value of the Cr^{3+} ions in the ground state is considerably smaller than $S = 3/2$. On the other hand, at lower fields ($B < 5000$ G), the abrupt approach of M to its maximum value is reminiscent of magnet behaviour. These peculiarities rapidly disappear at $T \geq 5$ K.

This anomalous magnetic behaviour of **1** below 5 K can be related to the zero-field splitting of the $^4A_{2g}$ ground spin state ($S = 3/2$) of Cr^{3+} ions. In distorted $[Cr(CN)_6]^{3-}$ com-

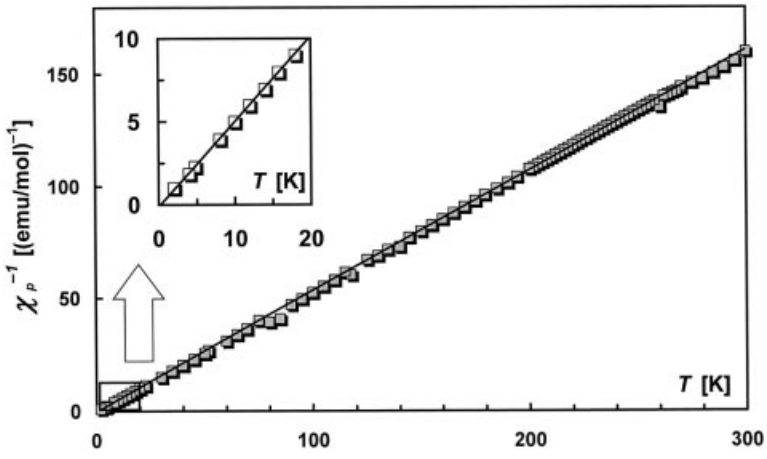

Figure 7. Temperature dependence of the reciprocal paramagnetic susceptibility, χ_p^{-1}(T), at 10 kG for $[RuNO(NH_3)_5][Cr(ox)_3]\cdot 3H_2O$. The inset shows the low temperature segment following the Curie–Weiss law with $C = 1.98$ emu K mol^{-1} and $\Theta = 0.26$ K.

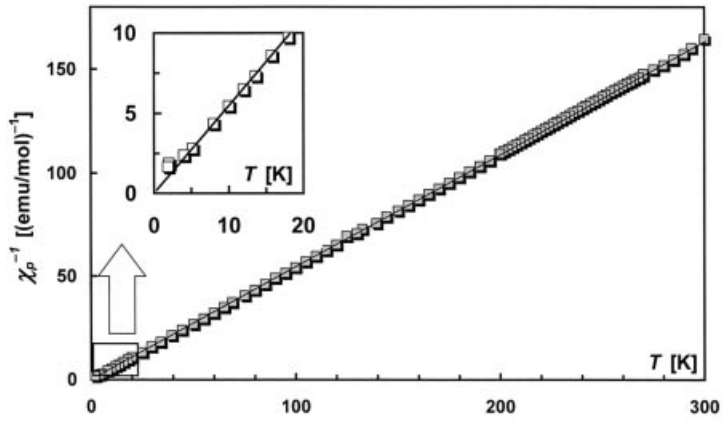

Figure 8. Temperature dependence of the reciprocal paramagnetic susceptibility, $\chi_p^{-1}(T)$, at 10 kG for $[RuNO(NH_3)_5][Cr(CN)_6]$. The inset shows the low temperature segment following the Curie–Weiss law with $C = 1.86$ emu K mol^{-1} and $\Theta = 0.18$ K.

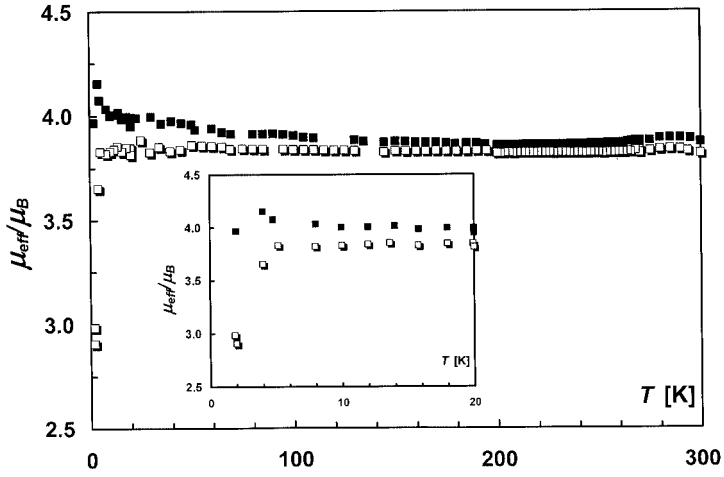

Figure 9. Temperature dependence of the effective magnetic moments of $[RuNO(NH_3)_5][Cr(ox)_3]\cdot 3H_2O$ (filled squares) and $[RuNO(NH_3)_5][Cr(CN)_6]$ (open squares) microcrystals measured at cooling, $B = 10$ kG. The insert shows the low temperature segment.

plexes, the spin-orbit interaction combined with the low-symmetry crystal-field component splits the $^4A_{2g}$ ground spin state into two Kramers doublets separated by a gap of $2D$ zero-field splitting energy. As a result, at low temperatures ($kT < 2D$) the effective magnetic moment drops (from 3.83 to 2.91 μ_B, Figure 9) due to preferential thermal population of the lower Kramers doublet. In this case, the low-temperature limit of the effective magnetic moment μ_{eff} of $[Cr(CN)_6]^{3-}$ can be calculated as $\mu_{eff}^2 = g_{av}^2\mu_B^2 S(S+1)$, where $S = 1/2$, $g_{av}^2 = (g_1^2 + g_2^2 + g_3^2)/3$ and g_1, g_2 and g_3 refer to the anisotropic g-tensor of the effective spin ($S = 1/2$) associated with the lower Kramers doublet of the split $^4A_{2g}$ ground state. Though the g_1, g_2, g_3 g-tensor components of the lower Kramers doublet can vary considerably for different distortions of $[Cr(CN)_6]^{3-}$ cyano complexes (typically, $g_1 = 1.97$, $g_2 = 3.78$, $g_3 = 4.08$ and $g_1 = 1.24$, $g_2 = 1.59$, $g_3 = 5.55$), the g_{av} value is insensitive to the specific type of distortion ($g_{av} \approx 3.40$). Thus we obtained $\mu_{eff} = 2.95$ μ_B for the low-temperature magnetic moment of $[Cr(CN)_6]^{3-}$, which is remarkably close to the measured value of 2.91 μ_B (at 1.99 K, Figure 9). This is also consistent with the low-temperature field dependence of magnetisation in which the saturated magnetic moment of **1** is considerably smaller that that of **2**, Figure 10.

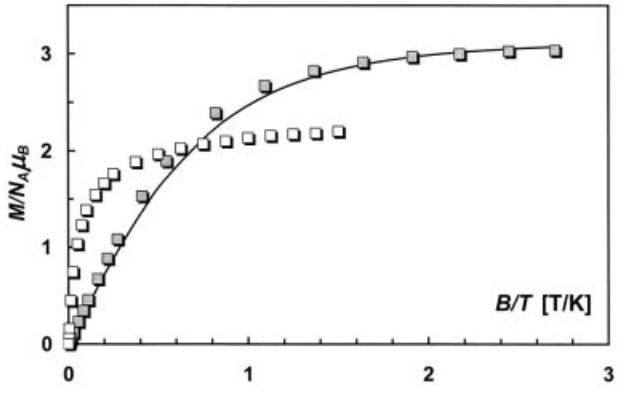

Figure 10. Field dependences of the magnetisation, $M/N_{A\mu B}$, of $[RuNO(NH_3)_5][Cr(ox)_3]\cdot 3H_2O$ (filled squares) and $[RuNO(NH_3)_5][Cr(CN)_6]$ (open squares) microcrystals at 1.83 K and 2.00 K, respectively. Measurements were carried out by decreasing the field down to 0 after field cooling at 50 kG and 30 kG, respectively. The solid curve denotes fitting by the Brillouin function with $S = 3/2$ and $g = 2.0800$. The experimental points are depicted with a normalised OX scale of B/T, unit G K^{-1}.

The zero-field splitting of $[Cr(CN)_6]^{3-}$ in **1** is approximately of the order $2D/k \approx 5$ K ($2D \approx 3$ cm^{-1}), as can be estimated from the onset of the drop of the magnetic moment of **1** (ca. 5 K, Figure 9). In most of Cr^{III} complexes (and Cr^{3+} ions doped in host lattices), the zero-field splitting of the $^4A_{2g}$ state is within 1 cm^{-1}. However, in some cases $2D$ can be considerably larger. This is especially true for complexes with ligands producing strong crystal-field splittings, such as cyanide ligands in $[Cr(CN)_6]^{3-}$ (in which the crystal-field splitting energy is as large as 26600 cm^{-1} [32]). It is important to note that the $2D$ splitting is sensitive to the strength of π-type metal–ligand interactions, which are especially strong for CN^- ligands.[33] Qualitative estimates of the $2D$ value (in terms of angular-overlap model calculations taking into account spin-orbit interaction, see ref.[34] for detail) indicate that for some hypothetical distortions of $[Cr(CN)_6]^{3-}$ complexes corresponding to the "frozen" crystal structure of **1** (Figure 2), the zero field splitting can reach a value of 3 cm^{-1} or even more.

On the other hand, an alternative explanation for the low-temperature magnetic behaviour of **1** in terms of through-space exchange interactions between paramagnetic $[Cr(CN)_6]^{3-}$ anions seems not to be reasonable since exchange interactions in **1** are expected to be very weak. This is evidenced from the fact that exchange interactions between Cr^{3+} ions involved in bulk and well-isolated complexes are generally quite small.[35,36] Thus, exchange interactions between isolated $[Cr(CN)_6]^{3-}$ complexes in a closely related compound $[Co(NH_3)_5(H_2O)]$ $[Cr(CN)_6]$ were found to be as small as $J = -0.03$ cm^{-1}.[35] A similar strength to the exchange interactions between $[Cr(NH_3)_6]^{3+}$ complexes can be found in $[Cr(NH_3)_6](ClO_4)_2Br{\cdot}CsBr$.[36] More detailed information on the low-temperature magnetic properties of $[RuNO(NH_3)_5][Cr(CN)_6]$ could be obtained from direct EPR and magnetic measurements for single crystals. Unfortunately, in contrast to the case of $[Co(NH_3)_5(H_2O)][Cr(CN)_6]$,[35] the sizes of the crystals of **1** obtained in our experiments were still too small for such measurements. The absence of these anomalies in the oxalate complexes **2** is consistent with a smaller zero-field splitting in $Cr(ox)_3$, ($2D \approx 0.9$ cm^{-1} ≈ 1.3 K.[37]).

Further information can be obtained from AC susceptibility measurements. The field dependences of the in-phase (χ'_M) and out-of-phase (χ''_M) AC susceptibility of $[RuNO(NH_3)_5][Cr(ox)_3]{\cdot}3H_2O$ and $[RuNO(NH_3)_5]$-$[Cr(CN)_6]$ are shown in Figure 11. We have not observed a maximum of χ'_M in the temperature dependences and this could be associated with the Curie constant. This indicates the absence of long-range order. However, the field dependences of χ''_M for $[RuNO(NH_3)_5][Cr(CN)_6]$ demonstrate a pronounced maximum of 3.46×10^{-2} emu mol^{-1} at 5200 G (note, that the X scale in Figure 11 is nonlinear). Similarly, χ'_M demonstrates an abrupt decrease in the same field range, $1500 < B < 23000$ G. Such behaviour is not typical of usual paramagnetic insulators. $[RuNO(NH_3)_5][Cr(ox)_3]{\cdot}3H_2O$ exhibits similar behaviour but with a much smaller out-of-phase susceptibility of 5.08×10^{-3} emu mol^{-1} at 5200 G. Taking into account spin dynamics, the experimental data presented in Figure 9 and Figure 10 can be interpreted as indicative of short-range magnetic ordering in both hexacyanide and oxalate complexes. This could not be explained in terms of the single-ion zero-field splitting effects only. Such behaviour for **1** is most likely due to weak exchange interactions between $[Cr(CN)_6]^{3-}$anions (which are expected to be of order 0.03 cm^{-1}, as is the case in $[Co(NH_3)_5(H_2O)]$-$[Cr(CN)_6]$[35]) combined with a rather strong (> 1 cm^{-1}) zero-field splitting of the $^4A_{2g}$ ground state and a statistical disorder of strongly distorted $[Cr(CN)_6]^{3-}$ cyano complexes (caused by the NO^+–CN^- coulombic interactions discussed above). In this case, magnetic interactions between strongly anisotropic ground Kramers doublets (effective spin $S = 1/2$) of Cr^{3+} ions can differ considerably from the conventional

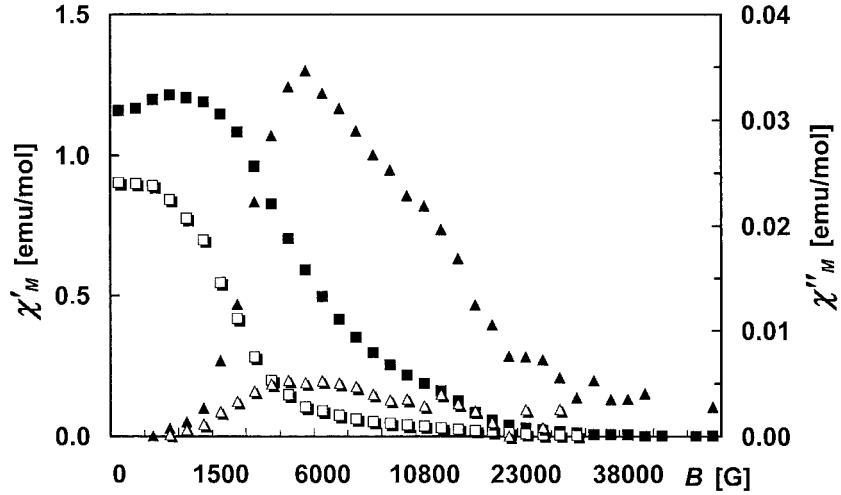

Figure 11. Field dependences of the AC magnetic susceptibilities of $[RuNO(NH_3)_5][Cr(ox)_3]{\cdot}3H_2O$ (open squares, open triangles) and $[RuNO(NH_3)_5][Cr(CN)_6]$ (filled squares, filled triangles) microcrystals measured at 1.81 K and 2.00 K, respectively. Solid squares denote the in-phase susceptibility, χ'_M, (filled and open symbols respectively, left axis) and solid triangles denote the out-of-phase susceptibility, χ''_M, (filled and open symbols respectively, right axis). The x axis has a nonlinear scale.

isotropic (Heisenberg) spin-spin coupling model [which is typical of the spin-only ($S = {}^3/_2$) $^4A_{2g}$ state of Cr^{3+} ions with a small zero-field splitting]. Interestingly, it has been found that the magnetic behaviour of a related compound $[Co(NH_3)_5(H_2O)][Cr(CN)_6]$ is compatible with the anisotropic Ising-type exchange interaction with $J = -0.18\ cm^{-1}$.[35] This value is consistent in magnitude with the paramagnetic Curie parameter $\Theta = 0.18$ K obtained for compound **1**. In principle, at low temperatures, this can lead to a spin-glass spin structure with strong local magnetic correlations caused by strongly anisotropic spin coupling. This might be responsible for the complicated low-temperature dynamic magnetic properties of **1** observed in our AC experiments. In contrast, AC magnetic characteristics of the oxalate compound are more compatible with the paramagnetic $S = {}^3/_2$ spin system with a small zero-field splitting. Further experiments on the AC susceptibility are in progress.

From the DSC experiments presented above one can conclude that the photochromic effect in $[RuNO(NH_3)_5][Cr(CN)_6]$ is stronger than that in $[RuNO(NH_3)_5][Cr(ox)_3]\cdot 3H_2O$. This result correlates with low-temperature magnetic measurements, according to which Cr^{3+} spins in hexacyanide complexes demonstrate a more pronounced dissipation to the lattice reservoir. This is generally consistent with a larger zero-field splitting of the $S = {}^3/_2$ ground spin state in $[Cr(CN)_6]^{3-}$ complexes, which provides a more efficient spin-lattice coupling.

Photomagnetic Properties

We measured the magnetic properties of **1** at 10 K and 5000 Oe while irradiating with blue light. Figure 12 shows the result of this photomagnetic experiment. Before irradiation, the $\chi_M T$ value was 1.89 emu mol^{-1} K. When the laser was switched on, thermal heating caused the sudden decrease of the magnetic signal, which then increased continuously until a plateau was reached after 8 h of light irradiation. When the laser was switched off, a sudden increase of the magnetic signal was observed due to the cessation of the thermal heating caused by the laser irradiation. The $\chi_M T$ value in the dark after the illumination was found to be 1.91 emu mol^{-1} K. Hence the light induces an increase of only 1% in the magnetic signal of compound **1**. This small effect is real and fully reversible, as was demonstrated by anneling the material at 300 K and then cooling again to 5 K whereby the original $\chi_M T$ value of 1.89 emu mol^{-1} K was measured again. The observation of such a weak photomagnetic effect is not really surprising, despite the fact that at 5 K the compound is in a photoexcited state. This may be interpreted as follows: the low-temperature metastable state is diamagnetic due to the $4d^6$ low-spin configuration of $RuNO(NH_3)_5$. In the irradiated compound, the NO ligand is rotated by about 180° from Ru–N–O (GS) to Ru–O–N (MSI). Hence, the coupling through hydrogen bonds to the paramagnetic $[Cr(CN)_6]$ anions changes with respect to the ground state as the attractive coulombic forces between the inverted NO (in MSI) and the CN^- differ from those between NO^+ and CN^- in GS. This indirect change of the electron density distribution in $[Cr(CN)_6]$ is the reason for the weak variation in the $\chi_M T$ value.

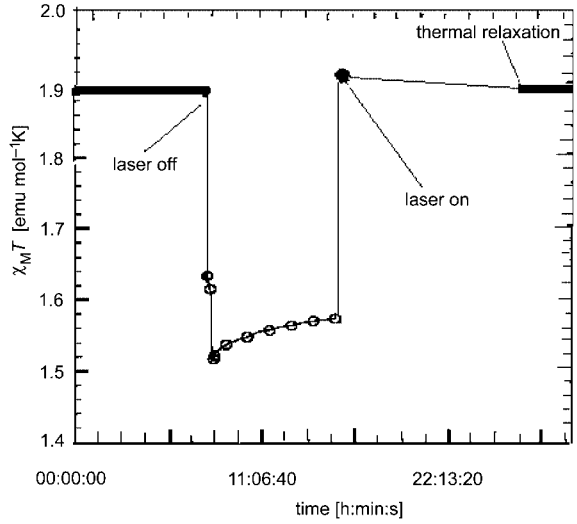

Figure 12. The time dependence of χ_MT before, during and after irradiation at 406–415 nm (P_{eff} = 10 mW cm^{-2}). The abrupt decreases are due to thermal effects when the laser is switched on.

Conclusions

The use of the photochromic mononitrosyl $[RuNO(NH_3)_5]^{3+}$ cation complex as a light sensitive building block for the preparation of functionalised paramagnets led to five new compounds: $[RuNO(NH_3)_5][Cr(CN)_6]$(**1**), $[RuNO(NH_3)_5][Fe(CN)_6]$(**2**), $[RuNO(NH_3)_5][Cr(ox)_3]\cdot 3H_2O$(**3**), $[RuNO(NH_3)_5][Fe(ox)_3]\cdot 3H_2O$(**4**) and $[RuNO(NH_3)_5][CrNO(CN)_5]$(**5**). The crystal structures of **1** and **3** are characterised by the presence of 3D networks of hydrogen bonds due to numerous N···N or N···O contacts between the CN (**1**) or ox (**3**) ligands of the anions and NH_3 ligands of the cations. The study of the photochromic properties of **1**–**5** showed that the anion's nature strongly affects the photochromism of the mononitrosyl Ru complex. In contrast to **1** and **3**, which exhibit reversible photochromic properties, the irradiation of **2** and **4** results in an irreversible photochemical reaction. Compound **5** composed of $[CrNO(CN)_5]^{3-}$ anions shows no photochromic behaviour. The study of the magnetic properties has shown that the paramagnetism of the complexes **1** and **3** is due to the Cr^{3+} spin system. No indications of the presence of a paramagnetic Ru^{III} oxidation state were found. The magnetic moment μ_{eff} of both complexes hardly changes in the temperature range from 300 K to 5 K. Below 5 K the μ_{eff} of $[RuNO(NH_3)_5][Cr(CN)_6]$ shows a pronounced decrease from 3.83 to 2.91 μ_B (at 1.99 K) whereas the μ_{eff} of $[RuNO(NH_3)_5][Cr(ox)_3]\cdot 3H_2O$ remains nearly constant. The field dependence of magnetisation for $[RuNO(NH_3)_5][Cr(ox)_3]\cdot 3H_2O$ is consistent with the model of noninteracting spins while the low-temperature behaviour of the field dependence of **1** is unusual and can not be explained

in terms of the Brillouin function. The anomalous magnetic behaviour of **1** below 5 K is due to both the zero-field splitting of the $S = {}^3/_2$ ground spin state of the Cr^{3+} ions and a weak exchange interaction between $[Cr(CN)_6]^{3-}$ anions. A weak reversible increase in the $\chi_M T$ value of **1** under light irradiation at low temperature has been observed.

Experimental Section

Materials: Chemicals: $H_2C_2O_4$, $FeCl_3$ (anhydrous), $K_3[M(CN)_6]$ (M = Cr, Fe), $K_3[Cr(ox)_3]$ and $(NH_4)_3[Fe(ox)_3]$ were used as purchased.

Syntheses

$[RuNO(NH_3)_5]Cl_3{\cdot}H_2O$: $[Ru(NH_3)_6]Cl_2$ (0.548 g, 2 mmol) synthesised as described in ref.[12] was dissolved in water (10 mL). 1 M HCl (10 mL) was added to the solution and then $NaNO_2$ (0.138 g, 2 mmol) was added in portions with continuous stirring. The resultant solution was heated in a water bath until intense gas evolution stopped. More $NaNO_2$ (0.069 g, 1 mmol) was then added to the cooled solution, which was then heated in a water bath until intense gas evolution stopped, concentrated to 10 mL, cooled and filtered from the $[RuNO(NH_3)_4Cl]Cl_2$ precipitate. The mother liquor was concentrated to ca. 2–3 mL, cooled and the $[RuNO(NH_3)_5]Cl_3{\cdot}H_2O$ precipitate was separated. The product was dissolved in 0.1 M HCl (4–5 mL), filtered from the $[RuNO(NH_3)_4Cl]Cl_2$ impurity and re-precipitated by addition of 96% ethanol (15–20 mL) to the mother liquor. The yield of purified $[RuNO(NH_3)_5]Cl_3{\cdot}H_2O$ was 516 mg (80%). $H_{17}N_6Cl_3O_2Ru$ (340.5): calcd. H 4.99, N 24.67, Cl 31.28; found H 4.98, N 24.09, Cl 31.21. IR: $\tilde{\nu}$ = 3432 (NH_3), 1928, 1913 (NO) cm^{-1}.

$[RuNO(NH_3)_5][Cr(CN)_6]$ (1): An aqueous solution (10 mL) of $K_3[Cr(CN)_6]$ (0.0487 g, 0.15 mmol) was added to an aqueous solution (5 mL) of $[RuNO(NH_3)_5]Cl_3H_2O$ (0.0511 g, 0.15 mmol). The yellow solution was allowed to stand for 2 d in the dark to form yellow-orange crystals. The crystals were collected by filter suction, washed with water and dried in vacuo over blue silica. The yield was 41.2 mg (65%). $C_6H_{15}N_{12}ORuCr$ (424): calcd. H 3.54, C 16.98, N 39.62; found H 3.50, C 17.03, N 39.98. IR: $\tilde{\nu}$ = 3432 (NH_3), 2199, 2127 (CN), 1947, 1914 (NO) cm^{-1}. Single crystals of quality suitable for X-ray diffraction analysis were selected from the synthetic sample.

$[RuNO(NH_3)_5][Fe(CN)_6]$ (2): The complex was prepared as a yellow powder in a similar way to the synthesis of **1** except that $K_3[Fe(CN)_6]$ was used instead of $K_3[Cr(CN)_6]$. The precipitate was formed immediately after mixing the solutions. The powder was collected by filter suction, washed with water and dried in vacuo over blue silica. The yield was 41.6 mg (65%). $C_6H_{15}N_{12}ORuFe$ (428.1): calcd. H 3.53, C 16.82, N 39.24; found H 3.80, C 17.03, N 39.17. IR: $\tilde{\nu}$ = 3449 (NH_3), 2112 (CN), 1944 (NO) cm^{-1}. Single crystals of quality suitable for X-ray diffraction were obtained by diffusion of the starting aqueous solutions into agar gel over 1.5 months.

$[RuNO(NH_3)_5][Cr(ox)_3]{\cdot}3H_2O$ (3): The compound was obtained as black hexagonal crystals in a synthesis similar to that of **1** except that $K_3[Cr(ox)_3]$ was used instead of $K_3[Cr(CN)_6]$. The yield was 86.8 mg (85%). $C_6H_{21}N_6O_{22}RuCr$ (682): calcd. H 3.58, C 12.29, N 14.33; found H 3.65, C 12.45, N 14.45. IR: $\tilde{\nu}$ = 3450 (NH_3), 1701 (C=O), 1918 and 1937 (NO) cm^{-1}. Single crystals of quality suitable for X-ray diffraction were selected from the synthetic sample.

$[RuNO(NH_3)_5][Fe(ox)_3]{\cdot}xH_2O$($x \approx 3$) (4): The complex was obtained as a yellow-orange powder in a synthesis similar to that used for **3** except that $(NH_4)_3[Fe(ox)_3]$ was used instead of $K_3[Cr(ox)_3]$. The precipitate was formed immediately after mixing the solutions. The yield was 80.1 mg (78%). $C_6H_{21}N_6O_{22}RuFe$ (686): calcd. H 3.56, C 12.20, N 14.24; found H 3.68, C 12.50, N 14.69. IR: $\tilde{\nu}$ = 3450 (NH_3), 1679 (C=O), 1914 (NO) cm^{-1}. Single crystals of quality suitable for X-ray diffraction analysis were prepared as follows: an aqueous solution (5 mL) of oxalic acid (0.27 g, 0.3 mmol) was added dropwise to a solution (5 mL) of $FeCl_3$ (anhydrous, 0.0163 g, 0.1 mmol) and an aqueous solution (5 mL) of $[RuNO(NH_3)_5]Cl_3{\cdot}H_2O$ (0.0341 g, 0.1 mmol) was then added. The yellow-orange solution was allowed to stand for 3 weeks in the dark to allow the formation of yellow-orange hexagonal crystals.

$[RuNO(NH_3)_5][CrNO(CN)_5]$ (5): An aqueous solution (5 mL) of $[RuNO(NH_3)_5]Cl_3{\cdot}H_2O$ was mixed with a solution of $K_3[CrNO(CN)_5]$ (1:1 equal molar ratio) and a powder precipitated. The yield was 51.2 mg (80%). $C_5H_{15}N_{12}O_2RuCr$ (428): calcd. H 3.15, C 14.02, N 39.24; found H 3.25, C 14.65, N 38.94. IR: $\tilde{\nu}$ = 3449 and 3440 (NH_3), 2118 (CN), 1936 (NO) cm^{-1}. Single crystals of quality suitable for X-ray diffraction were obtained by diffusion of the starting aqueous solutions into agar gel over 1.5 months.

Physical Measurements.

Spectra: Infrared spectra were recorded with a Perkin–Elmer spectrometer BX-2 in KBr pellets in the 4000-400 cm^{-1} region.

Crystallographic Data Collection and Structure Determination: Single crystals of **1** and **3** were mounted on an automatic four-circle KUMA DIFFRACTION diffractometer equipped with a graphite-monochromated Mo-K_α radiation source [$\omega/2\theta$ scanning, 2(θ) max = 80°]. The crystal structures were solved by direct methods using the SHELX-97[38] program package.The positions of hydrogen atoms were found evenly from the difference Fourier syntheses. The structures were refined in an anisotropic approximation excluding hydrogen atoms. The positions of the latter were refined in an isotropic approximation. The positions of N and O (NO) were determined from the difference Fourier synthesis. Since the position of N is a weighted average value between those of N (NH_3) and N (NO), it was used as a basic value in the refinement. The structures were refined using the restrained bond lengths by considering the occupancies of the positions of NH_3 and NO: Ru1–N1 1.75(0.03) Å, Ru1–N11 2.13(0.01) Å, N1–O1 1.22(0.01) Å. Crystallographic data are summarized in Table 1.

CCDC-602209 and -602210 (for compounds **1** and **3**) contain the supplementary crystallographic data for this paper. These data can be obtained free of charge from The Cambridge Crystallographic Data Centre via www.ccdc.cam.ac.uk/data_request/cif.

Differential Scanning Calorimetry (DSC): DSC measurements were performed using a modified differential scanning calorimeter (Mettler DSC 30, TA 3000) equipped with two quartz windows inside and outside the cryostat. The absolute calibration of enthalpy H and temperature T was controlled by measuring the phase-transition of In, Hg, pentane and KH_2PO_4. During illumination, the sample was kept at 120 K in a dry nitrogen atmosphere and subsequently heated at a constant heating rate $q = dT/dt = 5$ K/min. The exothermal heatflow is the time derivative of the enthalpy H. To obtain only the contribution of enthalpy of the metastable states, the enthalpy of the nonirradiated sample was subtracted from that of the irradiated one. The residual enthalpy was evaluated by fitting to the Arrhenius law modified for dynamic measurements.[10]

$$dH/dt = H_{tot}Z{\cdot}\exp[-\{(Z/q)\ {}_{T_0}\textstyle\int^{T}\exp(-E_A/k_BT) + (E_A/k_BT)\}]$$

(Z = frequency factor, E_A = activation energy, k_B = Boltzmann constant)

As a light source for generating MSI we used a metal-vapour lamp (HMI 575 Osram) filtered by dichroitic and interference filters to the spectroscopic range of 420–460 nm with the maximum at 434 nm. The intensity was 180 mW cm^{-2}. The irradiation time was 3 h which yielded an integrated flux of Q = 1944 J cm^{-2} on the sample. For the generation of MSII the samples were irradiated as described above and then irradiated with a Nd-YAG laser (1064 nm). The intensity was 138 mW cm^{-2}. The irradiation time was 0.5 h yielding an integrated flux of Q = 250 J cm^{-2}.

Magnetic and Photomagnetic Studies: The temperature and magnetic field dependences of the molar paramagnetic susceptibility, χ_P, magnetic moment in Bohr magnetons, $M/N_{A\mu B}$, effective magnetic moment, μ_{eff}/μ_B, and the in-phase (χ'_M) and out-of-phase (χ''_M) AC susceptibility of **1** and **3** were measured with a commercial SQUID magnetometer MPMS "Quantum Design". The temperature range was 1.8–300 K and the maximum magnetic field attained B = 5.0 T. AC susceptibility measurements were carried out at 80 Hz with modulation field amplitude of 4 G. Randomly oriented microcrystals of a typical weight of ca. 10 mg were put into a gel capsule. Typical cooling rates were 2 K min^{-1} for 300 K > T >200 K, 4 K min^{-1} for 200 K > T > 15 K and 1 K min^{-1} below 15 K. The background signal of a capsule was diamagnetic within the entire temperature range, not exceeding 16% (at 300 K) and 0.1% (at 1.98 K) of the sample signal. This was subtracted from the total signal. For field dependences, the signal from an empty capsule did not exceed 0.06%. The paramagnetic susceptibility was also corrected by taking into account the magnetic contributions of the ligands.

The photomagnetic experiments for **1** were performed with a Kr^+ laser coupled through an optical fibre directed into the SQUID cavity of the magnetometer working in the dc mode (MPMS-5S "Quantum Design"). Powdered samples of **1** were mounted on a sample holder as thin layers (weight 0.83 mg) to avoid surface effects during illumination. The mass was estimated based on the considering that at 5 K, the magnetisation after irradiation follows a Brillouin function for an S = $^3/_2$ spin. With this method and calculating a molecular weight at 424.37 g, the estimated mass of the sample is 0.83 mg. The samples were irradiated continuously over 8 hours using the multiline 406–415 nm under a magnetic field of 5 kOe at 10 K. The effective power of the light on the sample was measured to ca. 10 mW cm^{-2}. Magnetic properties ($\chi_M T$) were recorded before and after irradiation, in each case the light being turned off to avoid thermal inhomogeneities.[10]

Acknowledgments

We are grateful for the financial support of an RFBR grant No. 06-03-32433, the programme of RAS "Multifunctional materials", RAS grant No. 05-03-32384, NSH-1380.2003.2 and the DFG (Wo618/5-1).

[1] O. Sato, T. Iyoda, A. Fujishimi, K. Hashimoto, *Science* **1996**, *272*, 704.
[2] a) Z.-Z. Gu, O. Sato, T. Iyoda, K. Hashimoto, A. Fujishima, *J. Phys. Chem.* **1996**, *100*, 18289; b) Z.-Z. Gu, O. Sato, T. Iyoda, K. Hashimoto, A. Fujishima, *Mol. Cryst. Liq. Cryst.* **1996**, *286*, 147; c) Z.-Z. Gu, O. Sato, T. Iyoda, K. Hashimoto, A. Fujishima, *Chem. Mater.* **1997**, *9*, 1092.
[3] S. Ohkoshi, K. Hashimoto, *J. Am. Chem. Soc.* **1999**, *121*, 10591.
[4] a) O. Sato, Y. Einaga, A. Fujishima, K. Hashimoto, *Inorg. Chem.* **1999**, *38*, 4405; b) D. A. Pejakovich, J. L. Manson, J. S. Miller, A. J. Epstein, *Phys. Rev. Lett.* **2000**, *85*, 1994; c) A. Goujon, O. Roubeau, F. Varret, A. Dolbecq, A. Bleuzen, M. Verdaguer, *Eur. Phys. J.* **2000**, *B14*, 115.
[5] P. Gütlich, Y. Garcia, T. Woike, *Coord. Chem. Rev.* **2001**, *219–221*, 839.
[6] T. Hauser, V. Oestreich, H. D. Rohrweck, *Z. Phys. A* **1977**, *280*, 17.
[7] Th. Woike, W. Krasser, P. S. Bechthold, S. Haussühl, *Phys. Rev. Lett.* **1984**, *53*, 1767.
[8] P. Coppens, D. Fomichev, M. D. Carducci, K. J. Culp, *J. Chem. Soc. Dalton Trans.* **1998**, 865.
[9] Y. Morioka, A. Ishikawa, H. Tomizawa, E. Miki, *J. Chem. Soc. Dalton Trans.* **2000**, 781.
[10] D. Schaniel, Th. Woike, B. Delley, C. Boskovic, D. Biner, W. Krämer, H.-U. Güdel, *Phys. Chem. Chem. Phys.* **2005**, *7*, 1164.
[11] L. A. Kushch, L. S. Plotnikova, Yu. N. Shvachko, V. A. Emel′yanov, E. B. Yagubskii, G. V. Shilov, S. M. Aldoshin, *J. Phys. IV Fr.* **2004**, *114*, 459.
[12] F. M. Lever, A. R. Powell, *J. Chem. Soc. (A)* **1969**, *9*, 1477.
[13] P. Coppens, I. Novozhilova, A. Kovalevsky, *Chem. Rev.* **2002**, *102*, 861.
[14] J. A. Olabe, L. A. Gentil, G. Rigotti, A. Navaza, *Inorg. Chem.* **1984**, *23*, 4297.
[15] D. Schaniel, Th. Woike, J. Schrefer, V. Petrichek, *Phys. Rev. B* **2005**, *71*, 174112.
[16] E. A. Bruker, J. S. Olson, M. Ikeda-Saito, G. N. Phillips, *J. Proteins: Struct. Function, Genetics* **1998**, *30*, 352.
[17] R. Feltham, J. Enemark, in *Topics in Inorganic and Organometallic Stereochemistry* (Ed.: G. Geoffroy), Wiley-VCH, New York, USA, **1981**, 155–215.
[18] S. I. Gorelsky, A. B. P. Lever, *Int. J. Quant. Chem.* **2000**, *80*, 636.
[19] S. C. Da Silva, D. W. Franco, *Spectrochim. Acta Part A* **1999**, *55*, 1515.
[20] M. E. Sanchez, M. L. Doublet, C. Faulmann, I. Malfant, P. Cassoux, L. A. Kushch, E. B. Yagubskii, *Eur. J. Inorg. Chem.* **2001**, 2797.
[21] J. T. Veal, D. J. Hodgson, *Inorg. Chem.* **1972**, *11*, 1420.
[22] Y. N. Mikhailov, A. S. Kanishcheva, A. A. Svetlov, *Zh. Neorg. Khim.* **1989**, *34*, 2803.
[23] H. J. Choi, J. J. Sokol, J. R. Long, *Inorg. Chem.* **2004**, *43*, 1606.
[24] F. Bottomley, *J. Chem. Soc. Dalton Trans.* **1997**, 1600.
[25] T. Woike, W. Krasser, H. Zöllner, W. Kirchner, S. Z. Haussühl, *Phys. D* **1993**, *351*, 25.
[26] H. Zöllner, W. Krasser, Th. Woike, *Chem. Phys. Lett.* **1989**, *161*, 497.
[27] T. Woike, H. Zöllner, W. Krasser, S. Haussühl, *Solid State Comm.* **1990**, *73*, 149.
[28] T. Woike, S. Haussühl, *Solid State Comm.* **1993**, *86*, 333.
[29] K. Ookubo, Y. Morioka, H. Tomizawa, E. J. Miki, *Mol. Struct.* **1996**, *379*, 241.
[30] D. Schaniel, T. Woike, C. Boskovich, H.-U. Güdel, *Chem. Phys. Lett.* **2004**, *390*, 347.
[31] D. Schaniel, T. Woike, L. Tsankov, M. Imlau, *Thermochim. Acta* **2005**, *429*, 19.
[32] B. N. Figgis, P. A. Reynolds, *Inorg. Chem.* **1985**, *24*, 1864.
[33] L. E. Mohrmann, B. B. Garrett, *Inorg. Chem.* **1974**, *13*, 357.
[34] D. Gatteschi, L. Sorace, *Solid State Chem.* **2001**, *159*, 253.
[35] P. A. Reynolds, C. D. Delfs, B. N. Figgis, B. Moubaraki, K. S. Murray, *Austr. J. Chem.* **1992**, *45*, 1899.
[36] R. D. Chirico, R. L. Carlin, *Inorg. Chem.* **1980**, *19*, 3031.
[37] L. S. Singer, *J. Chem. Phys.* **1955**, *23*, 379.
[38] G. M. Sheldrick, *SHELX97, Program for Crystal Structure Refinement*, University of Göttingen, Germany, **1997**

Received: March 28, 2006
Published Online: August 21, 2006

